Biophysical Journal Volume 86 February 2004 1089–1104

Adenylation-Dependent Conformation and Unfolding Pathways of the NAD$^+$-Dependent DNA Ligase from the Thermophile *Thermus scotoductus*

Daphné Georlette,*,** Vinciane Blaise,* Fabrice Bouillenne,† Benjamin Damien,‡ Sigridur H. Thorbjarnardóttir,§ Eric Depiereux,‡ Charles Gerday,* Vladimir N. Uversky,¶‖ and Georges Feller*

*Laboratory of Biochemistry, Institute of Chemistry B6, University of Liège, B-4000 Liège, Belgium; †Laboratoire d'Enzymologie et Centre d'Ingénierie des Protéines, Institute of Chemistry B6, University of Liège, B-4000 Liège, Belgium; ‡Unité de Biologie Moléculaire, Département de Biologie, Facultés Universitaires Notre-Dame de la Paix, B-5000 Namur, Belgium; §Laboratory of Molecular Genetics, Institute of Biology, University of Iceland, Grensasvegur 12, IS-108 Reykjavik, Iceland; ¶Institute for Biological Instrumentation, Russian Academy of Sciences, Pushchino, Moscow Region 142290, Russia; ‖Department of Chemistry and Biochemistry, University of California, Santa Cruz, California 95064; and **Department of Molecular and Cell Biology, University of California, Berkeley, California 94720-3204

ABSTRACT In the last few years, an increased attention has been focused on NAD$^+$-dependent DNA ligases. This is mostly due to their potential use as antibiotic targets, because effective inhibition of these essential enzymes would result in the death of the bacterium. However, development of an efficient drug requires that the conformational modifications involved in the catalysis of NAD$^+$-dependent DNA ligases are understood. From this perspective, we have investigated the conformational changes occurring in the thermophilic *Thermus scotoductus* NAD$^+$-DNA ligase upon adenylation, as well as the effect of cofactor binding on protein resistance to thermal and chemical (guanidine hydrochloride) denaturation. Our results indicate that cofactor binding induces conformational rearrangement within the active site and promotes a compaction of the enzyme. These data support an induced "open-closure" process upon adenylation, leading to the formation of the catalytically active enzyme that is able to bind DNA. These conformational changes are likely to be associated with the protein function, preventing the formation of nonproductive complexes between deadenylated ligases and DNA. In addition, enzyme adenylation significantly increases resistance of the protein to thermal denaturation and GdmCl-induced unfolding, establishing a thermodynamic link between ligand binding and increased conformational stability. Finally, chemical unfolding of deadenylated and adenylated enzyme is accompanied by accumulation of at least two equilibrium intermediates, the molten globule and premolten globule states. Maximal populations of these intermediates are shifted toward higher GdmCl concentrations in the case of the adenylated ligase. These data provide further insights into the properties of partially folded intermediates.

INTRODUCTION

DNA ligases are ubiquitous enzymes required for important cellular processes such as DNA replication, DNA recombination, and DNA repair, in all three kingdoms of life (Lehman, 1974). They are divided into two broad classes, those requiring NAD$^+$ as cofactor and those requiring ATP (Lehman, 1974). Regardless of their energy source, they catalyze the sealing of 5′-phosphate and 3′-hydroxyl termini at nicks in duplex DNA by means of three distinct catalytic events (Lehman, 1974). The first involves activation of the ligase through the formation of a covalent adenylated intermediate by transfer of the adenyl group of NAD$^+$ or ATP to the ε-NH_2 of a conserved lysine residue in the DNA ligase. In the second step, the AMP moiety is transferred from the ligase to the 5′-phosphate group at the single-strand break site, creating a new pyrophosphate bond. Finally, DNA ligase catalyzes the DNA ligation step with loss of free AMP.

NAD$^+$-dependent ligases are of fairly uniform size (~70 kDa) and display extensive amino acid sequence conservation throughout the entire protein. They are composed of four discrete domains (Doherty and Suh, 2000; Lee et al., 2000). Domain 1 comprises the subdomain 1a, required for ligase adenylation (Sriskanda and Shuman, 2002) and the subdomain 1b, called "Adenylation domain," containing the lysine residue implicated in enzyme adenylation. The domain 2 is called "Oligomer-Binding (OB) fold domain." The domain 3 contains a zinc finger (subdomain 3a) and a HhH (Helix-hairpin-Helix) (subdomain 3b) subdomains, whereas the domain 4 consists of a "BRCT domain" (BRCA-carboxy-terminal-related domain). ATP-dependent ligases are more diverse in size but share a common ligase domain (formed by domains 1 and 2) called "catalytic core." This domain comprises six conserved sequence motifs, I, III, IIIa, IV, V-VI, that define a family of related nucleotidyltransferases including mRNA capping enzymes as well as RNA- and tRNA-ligases (Hakansson et al., 1997). Some ATP ligases are possibly flanked by additional domains that are likely to be implicated in the enzyme specialization, targeting the various ATP DNA ligases to different pathways in DNA repair and replication (for review, see Martin and

Submitted July 9, 2003, and accepted for publication September 22, 2003.

Address reprint requests to Georges Feller, Laboratory of Biochemistry, Institute of Chemistry B6, University of Liège, B-4000 Liège, Belgium. Tel.: +32-4-366-33-43; Fax: +32-4-366-33-64; E-mail: gfeller@ulg.ac.be.

Abbreviations used: AEW, average emission wavelength; ANS, 8-anilino-1-naphtalene sulfonic acid; GdmCl, guanidine hydrochloride; FI, fluorescence intensity; FPLC, fast protein liquid chromatography; NAD$^+$, nicotinamide adenine dinucleotide; NMN, nicotinamide mononucleotide; MG, molten globule; PMG, premolten globule; SEC, size exclusion chromatography; *Ts*lig, *Thermus scotoductus* DNA ligase.

0006-3495/04/02/1089/16 $2.00

MacNeill (2002); Timson et al. (2000)). Although there is a scant amino acid sequence similarity between NAD^+- and ATP- DNA ligases, the tertiary structures of the catalytic cores are quite well conserved (Doherty and Suh, 2000; Singleton et al., 1999; Timson et al., 2000) and the adenylate binding pocket of NAD^+ ligases is composed of the same six nucleotidyl transferase motifs described originally in the ATP-dependent enzymes (Aravind and Koonin, 1999). The conservation and similarity of these structural features strongly suggest that the two types of ligases have evolved from a common ancestor and are likely to have a similar catalytic mechanism. The divergence may have largely arisen from the need to accommodate different nucleotide cofactors (Aravind and Koonin, 1999).

Nick recognition requires ligases to be adenylated at the lysine residue located within the active site (Shuman, 1995). In fact, molecular modeling studies of T7 DNA ligase suggest that dsDNA binds predominantly in a positively charged interdomain cleft, between domain 1 and 2 (Doherty and Dafforn, 2000). Upon adenylation, the DNA binding domain 2, rotates around and exposes the DNA-binding face toward the active site (closed conformation), allowing DNA to bind. In the deadenylated enzyme, the proposed DNA-binding face is rotated away from the active site cleft (open conformation). Therefore, adenylation would act as a conformational switch, facilitating rotation of the DNA-binding surface of the OB fold toward the active site cleft. In this view, only adenylated ligase can bind to nicked DNA, preventing the formation of nonproductive ligase-DNA complexes. Interestingly, two crystal structures of PBCV-1 mRNA capping enzyme have provided conclusive evidence for such open-closed conformational switch during the guanylylation reaction (Hakansson et al., 1997), which is equivalent to the adenylation reaction catalyzed by DNA ligases (Shuman and Schwer, 1995). This involves a 13-Å movement of the C-terminal OB domain 2 toward domain 1. Such conformational modification has also been proposed for the *Thermus filiformis* NAD^+-DNA ligase (Lee et al., 2000). In this case, domain 4 (BRCT domain) is very mobile in the open conformation but its mobility is restricted in the closed conformation, allowing a contact with domain 1a, which leads to an active toroidal conformation (Lee et al., 2000). Thus, despite their different amino acid sequences and specificities, all these enzymes are likely to undergo major domain rearrangements upon cofactor binding.

To date, NAD^+-dependent DNA ligases have been predominantly isolated from eubacteria (Wilkinson et al., 2001). For that reason, they constitute an attractive target for broad-spectrum antibiotic therapy predicated on blocking the reaction of DNA ligase with NAD^+, leading to an inactive enzyme and thus growth arrest of the eubacterium. The drug-binding site would ideally be unique to, and conserved among, NAD^+-DNA ligases but absent from ATP-dependent ligases and other essential NAD^+-requiring enzymes. This strategy implies that: i), the conformational modifications involved in the catalysis of NAD^+-dependent DNA ligases are understood and ii), the structural components of NAD^+-ligases interacting specifically with NAD^+ are known. A recent study, in which the role of domain Ia of *Escherichia coli* DNA ligase was investigated, has provided major advances toward the elucidation of this later issue (Sriskanda and Shuman, 2002). This domain, essential for the reaction with NAD^+ and unique to NAD^+-dependent ligases, contains several conserved residues likely interacting with the nicotinamide mononucleotide (NMN) moiety of the NAD^+ substrate. Because this domain is well conserved among all NAD^+-ligases, it is expected that the role of domain Ia is common to all of them. To characterize the structural changes occurring upon adenylation, we have investigated the unfolding pathways of the deadenylated and adenylated *Thermus scotoductus* DNA ligase (*Ts*lig). This enzyme possesses all the conserved motifs common to NAD^+-dependent ligases and shows similar overall catalytic properties to other NAD^+-dependent DNA ligases (Thorbjarnardóttir et al., 1995). In this paper, we show that cofactor binding induces conformational changes within the active site of *Ts*lig, suggesting an open-closure mechanism upon adenylation. In addition, we provide strong evidences that cofactor binding also induces increased resistance to thermal and chemical denaturation. Finally, the results of chemical denaturation analysis indicate that the unfolding is a complex sequential process and goes through at least two intermediates, the molten globule and pre-molten globule states.

MATERIALS AND METHODS

Chemicals and enzymes

3-(1-pyridinio)-1-propane sulfonate and acrylamide were from Fluka (Buchs, Switzerland) β-NAD^+, β-NMN, and 8-anilino-1-naphtalene sulfonic acid (ANS) were from Sigma-Aldrich NV/SA (St. Louis, MS). Guanidine Hydrochloride (GdmCl, ultra pure) was from ICN Biomedicals Inc. (Irvine, CA). Hi-Trap Heparin, MonoQ HR 5/5, Superdex 200 HR 10/30, and fast protein liquid chromatography (FPLC) systems were from Pharmacia LKB Biotechnology (Stockholm, Sweden). Water used for the experiments was purified over a Milli-Q water purification system from Millipore (Billerica, MA), and all solutions were filtered through 0.22 μm filters before use. Plasmid encoding *T. scotoductus* NAD^+-DNA ligase (*Ts*lig) was a kind gift from Z. O. Jónsson and G. Eggertsson (Reykjavik, Iceland) (Thorbjarnardóttir et al., 1995).

Three-dimensional modeling

The target sequence for modeling is the NAD^+-dependent DNA ligase from *T. scotoductus*. The modeling, minimizations, and molecular dynamics were done using the molecular operating environment (MOE) program (Chemical Computing Group, Montreal, Canada). Optimal multiple sequence alignment was performed using the Match-Box program (Depiereux et al., 1997). The first step was a Protein Data Bank search using the target sequence to find the templates with the highest homology. Originally, a fast scan was performed using the Fasta methodology (Pearson, 1996). An expectation value (E-Value) was determined for each sequence. Then, the list was reduced using thresholds of the E-value (E-Value Cutoff and E-Value Accept). Only E-Values lower than E-Value Cutoff and with *Z*-score higher than 7 were accepted.

The best template found for *T. scotoductus* was 1DGS.A, the homologous NAD^+-DNA-ligase of *Thermus filiformis* (expected value: $7.2\ 10^{-259}$), which does not contain a C-terminal BRCT domain (Lee et al., 2000). The five best templates were then aligned using the Match-Box software and evaluated using secondary structure prediction algorithm. The alignment was then introduced into the modeling process. Thus, 1DGS.A was used as a template for the modeling. The modeling program was configured to include outgaps and to build 10 intermediate models using a Boltzmann-weighted randomized modeling procedure adapted from Levitt (1992), combined with specialized logic for the proper handling of insertions and deletions (Fechteler et al., 1995), minimize them, and select the best intermediate. The final model is the one that scored best according to the packing quality function. The obtained model was then thoroughly minimized, using steepest gradient algorithm for 100 iterations, followed by the conjugate gradient algorithms for another 100 iterations, to end with the truncated Newton algorithm until the root-mean-square gradient went under 0.01.

The obtained model was then reviewed following the experimental data for the homologous proteins, and using MOE's stereochemical quality evaluation tools to confirm that the model's stereochemistry is reasonably consistent with the typical values found in crystal structures.

At this step a molecular dynamics was done using Molarity, Volume, Temperature thermodynamic ensemble (number of particles, volume, and temperature are fixed). The equilibrium temperature chosen was 354°K, known as the optimal temperature of *T. scotoductus*. The heating, equilibrium, and cooling cycles were held for 1000 iterations each. The most stable conformation was chosen as a final model.

Protein purification

The recombinant wild-type *T. scotoductus* NAD^+-DNA ligase (*Ts*lig) was overexpressed as previously described (Thorbjarnardóttir et al., 1995), except that the growth was performed in TB medium (12 g/l tryptone, 24 g/l yeast extract, 4 ml/l glycerol, 12.54 g/l K_2HPO_4, 2.32 g/l KH_2PO_4 pH 7) containing 100 μg/ml ampicillin. *Ts*lig DNA ligase was purified by two successive heatings (65°C and 80°C), followed by Hi-Trap Heparin and MonoQ HR chromatographic steps. Protein concentration was determined with the Coomassie protein assay reagent (Pierce, Rockford, IL), using BSA as standard. The final yield was ~55 mg of protein per liter of culture. N-terminal sequencing confirmed the integrity of the recombinant protein. As previously reported in literature for NAD^+-dependent DNA ligases (Barany and Gelfand, 1991; Brannigan et al., 1999; Georlette et al., 2000; Ishino et al., 1986; Kaczorowski and Szybalski, 1996; Modrich et al., 1973; Panasenko et al., 1978; Singleton et al., 1999; Takahashi and Uchida, 1986; Zimmerman and Pheiffer, 1983), the native recombinant enzyme is produced in an adenylated form: DSC, fluorescence, and circular dichroism profiles of the native and adenylated *Ts*lig (after incubation with NAD^+) are superimposable.

Deadenylation/adenylation of *Ts*lig

*Ts*lig stock solution was either deadenylated or adenylated according to Timson (Timson and Wigley, 1999) by adding excess of β-NMN or β-NAD^+, respectively. The ratio [NMN/NAD^+]/[*Ts*lig] was ~80. Deadenylated/adenylated mixtures were then heated at 65°C for 30 min and then cooled rapidly on ice. When required, protein solutions were dialyzed against appropriate buffer before experiments.

Differential scanning calorimetry

Measurements were performed using a MicroCal MCS-DSC instrument at a scan rate of 60 K/h and under 2 atm nitrogen pressure. Samples (~4 mg/ml) were dialyzed overnight against 30 mM MOPS, 50 mM KCl, pH 7.6. To decrease aggregation, a nondetergent sulphobetaine (3-(1-pyridinio)-1-propane sulfonate) was added before differential scanning calorimetry (DSC) experiment (Goldberg et al., 1995), to a final concentration of 0.75 M. Thermograms were analyzed according to a non-two-state model in which T_m, ΔH_{cal}, and ΔH_{eff} of individual transitions are fitted independently using the MicroCal Origin software (version 2.9). The magnitude and source of the errors in the T_m and enthalpies values have been discussed elsewhere (Matouschek et al., 1994). All scans were found to be irreversible under the experimental conditions used for these studies.

GdmCl-induced unfolding transitions

*Ts*lig deadenylated/adenylated samples were incubated overnight at 25°C in the presence of various concentrations of guanidine hydrochloride (GdmCl). Unfolding curves were determined by monitoring the intrinsic fluorescence emission or circular dichroism (CD) at 25°C. The pH was checked to ensure a constant value throughout the whole transition, and the denaturant concentration was determined from refractive index measurements (Pace, 1986), using a R5000 hand refractometer from Atago (Tokyo, Japan).

Fluorescence measurements

Both intrinsic and ANS fluorescence emission spectra were recorded on an Aminco SLM 8100 spectrofluorimeter. Excitation and emission slit widths were 2 and 4 nm, respectively, and the scan speed was 350 nm/min. Cuvettes with 1-cm pathlength were used. Intrinsic fluorescence measurements were performed using a protein concentration of 25 μg/ml (0.33 μM), with excitation at 280 nm, and emission spectra recorded from 300 to 440 nm. The buffer used was 20 mM phosphate sodium, 50 mM NaCl, pH 7.6, in the presence of desired GdmCl concentrations. With all samples, fluorescence spectra were corrected for the background fluorescence of the solution (buffer + denaturant). Two fluorescence parameters have been considered in this work: the fluorescence intensity at single excitation and emission wavelengths and the average emission wavelength (AEW). The AEW values were computed according to the following equation (Royer et al., 1993),

$$AEW = \frac{\sum_{i=\lambda 1}^{\lambda N} (F_i \times \lambda_i)}{\sum_{i=\lambda 1}^{\lambda N} (Fi)}, \quad (1)$$

where F is the fluorescence intensity and λ the wavelength. The AEW values were calculated between 300 and 440 nm.

ANS fluorescence measurements were performed with the samples used for intrinsic fluorescence measurements, with excitation at 390 nm, and emission spectra recorded from 420 to 600 nm. The fluorescence spectra were corrected for the background fluorescence of ANS. The ratio [ANS]/[*Ts*lig] was ~250 ($\varepsilon_{350nm} = 4950\ M^{-1}\ cm^{-1}$ for ANS).

Circular dichroism measurements

Circular dichroism (CD) spectra were recorded at 25°C using a CD6 Jobin Yvon spectropolarimeter under constant nitrogen flow. In the far ultraviolet (UV) region, spectra were recorded in a 0.1-cm cell at protein concentrations of ~0.25 mg/ml whereas in the near UV region, a 1.0-cm cell was used for protein concentrations of ~1 mg/ml. The buffer used was 20 mM sodium phosphate, 50 mM NaCl, pH 7.6, in the presence of desired GdmCl concentrations. Spectra were acquired at a scan speed of 20 nm/min, with a 2-nm bandwidth and a 1-s integration time. Spectra were averaged over five scans and corrected for the buffer signal. Raw data were expressed in terms of the mean residue ellipticity [θ] using the known mature adenylated *Ts*lig sequence (MW = 76855 Da) for calculation of the mean residue weight.

GdmCl unfolding curves of adenylated *Ts*lig were recorded at 222 and 280 nm, using a 2-nm bandwidth. At all denaturant concentrations, at least 30 data points were acquired over 1 min (2-s integration time), and averaged.

The resulting values were corrected for the contribution of the solvent. An estimate of the helical content (f_H) of *Ts*lig has been obtained from the following equation (Chen et al., 1972),

$$[\theta]_{222} = (-30300 \times f_H) - 2340, \quad (2)$$

where $[\theta]_{222}$ is the mean residue ellipticity (deg cm^2 dmol^{-1}) at 222 nm.

Data analysis

The transition curves obtained by fluorescence spectroscopy and CD were analyzed using Eqs. 3 and 4, assuming a two- (N↔U, where N is the native state and U is the fully unfolded state) or three-state model (N↔I↔U, where I is the thermodynamically stable intermediate) for the unfolding reaction. For N↔U transition (Pace, 1990),

$$y_{obs} = \{(y_N + p \times [D]) + (y_U + q \times [D])\exp[a]\}/(1 + \exp[a]), \quad (3)$$

where

$$a = (-\Delta G_{(H2O)} + m \times [D])/RT,$$

and where y_{obs} is the measured variable parameter at a given denaturant concentration, whereas y_N and y_U represent the values of this parameter for the native and denatured states, respectively. $\Delta G_{(H2O)}$ is the difference in free energy between folded and unfolded conformations under physiological concentrations and m is a measure of the dependence of the free energy on the denaturant concentration [D]; p and q are the slopes of the pre- and post-unfolding baselines, respectively, R is the gas constant and T is the absolute temperature. The midpoint of the denaturation curve ([U]/[N] = 1) is given by $C_m = \Delta G_{(H2O)}/m$. For N↔I↔U process (Vanhove et al., 1997),

$$y_{obs} = \{(y_N + p \times [D]) + y_I\exp[a] + y_U\exp[a]\exp[b]\} /(1 + \exp[a] + \exp[a]\exp[b]), \quad (4)$$

where

$$a = (-\Delta G_{N-I}(H_2O) + m_{N-I} \times [D])/RT \text{ and}$$
$$b = (-\Delta G_{I-U}(H_2O) + m_{I-U} \times [D])/RT,$$

and where $\Delta G_{N\text{-}I}(H_2O)$ and $\Delta G_{I\text{-}U}(H_2O)$ are the differences in free energy between I and N and between U and I, respectively, in the absence of denaturant, and $m_{N\text{-}I}$ and $m_{I\text{-}U}$ are the slopes of the transitions.

Analysis of circular dichroism data using the "phase diagram" method

The ''phase diagram'' method analysis of spectroscopic data is extremely sensitive for the detection of intermediate states (Burstein, 1976; Bushmarina et al., 2001; Kuznetsova et al., 2002; Munishkina et al., 2003; Permyakov et al., 1980; Uversky et al., 2003). Although this method was developed for the analysis of fluorescence data (Burstein, 1976), it can be used with any spectroscopic technique. The essence of this method is to build up the diagram of $I_{\lambda 1}$ vs. $I_{\lambda 2}$, where $I_{\lambda 1}$ and $I_{\lambda 2}$ are the spectral intensity values measured at wavelengths $\lambda 1$ and $\lambda 2$ under different experimental conditions for a protein undergoing structural transformations. The relationship between $I_{\lambda 1}$ and $I_{\lambda 2}$ is described in the following equation,

$$I_{(\lambda 1)} = a + (b \times I_{(\lambda 2)}). \quad (5)$$

The calculations allowing the determination of such equation, as well as the composition of a and b can be found elsewhere (Kuznetsova et al., 2002; Uversky et al., 2003). As a rule, $\lambda 1$ and $\lambda 2$ are arbitrary wavelengths of the spectrum, but in practice, such diagrams will be more informative if $\lambda 1$ and $\lambda 2$ will be on different slopes of the spectrum. If the wavelengths are from one slope or near the maximum, some transitions may remain undetected.

Size exclusion chromatography

Hydrodynamic dimensions (Stokes radius, R_S) of deadenylated and adenylated *Ts*lig in different conformational states were measured by gel filtration. Size exclusion chromatography (SEC) was performed on the Superdex 200 H/R 10/30 prepacked FPLC column calibrated according to (Uversky, 1993). Protein (~0.25 mg/ml) containing the required concentrations of GdmCl was loaded onto the column equilibrated with the same buffer. The elution was carried out isocratically at a flow rate of 1.0–0.5 ml/min and monitored by the absorbance at 280 nm. All measurements were made at 25°C. Molecular Stokes radii (R_S) were estimated from elution volume V^{el} measured according to the following equation,

$$R_S = \frac{(1000/V^{el}) - 42.44}{0.9114}. \quad (6)$$

The accuracy of determination of R_S by this equation is ~95%. Relative areas of chromatographic peaks were estimated from the elution profiles by their deconvolution using LabCalc. The accuracy of such deconvolution was ~90%. Stages of unfolding of *Ts*lig were determined as follows (Uversky and Ptitsyn, 1994, 1996),

$$f_{LC} = S_{LC}/(S_C + S_{LC}), \quad (7)$$

where f_{LC} represents the fraction of molecules that undergoes the transition from a compact (C) to a less compact state and is determined from relative areas (S) of corresponding FPLC peaks

$$f_U = f_{LC}[(\langle V^{el}_{LC}\rangle - V^{el}_{PMG})/(V^{el}_U - V^{el}_{PMG})], \quad (8)$$

where f_U represents the fraction of unfolded molecules, and where $\langle V^{el}_{LC}\rangle$, V^{el}_{PMG}, and V^{el}_U are the average elution volume of less compact molecules, the elution volume of molecules in the premolten globule state, and the elution volume of molecules in the unfolded state, respectively.

$$f_N = 1 - f_D$$
$$f_{MG} = f_D - f_{LC}$$
$$f_{PMG} = f_{LC} - f_U \quad (9)$$

where f_N, f_{MG}, f_{PMG}, and f_U are the fraction of molecules in native, molten-globule, premolten globule, and unfolded states, respectively.

Stern-Volmer quenching

The conformational state of enzymes was further characterized by acrylamide-induced fluorescence quenching. Samples were prepared in 20 mM sodium phosphate buffer, 50 mM NaCl, pH 7.6, and the protein concentrations were adjusted to provide an optical density at the excitation wavelength <0.1. Aliquots of a 1.2-M acrylamide stock solution were consecutively added to 1 ml protein solution to increase acrylamide concentration by ~5 mM steps. Experiments were performed using excitation at 295 nm with fluorescence emission set at 333 nm (excitation and emission slit widths were 1 and 4, respectively) and the fluorescence intensities were recorded for 30 s. Experiments were performed in triplicate. The data were corrected for the dilution effects and for the absorptive screening caused by acrylamide ($\varepsilon_{295nm} = 0.25$ M^{-1} cm^{-1} for acrylamide). Quenching data were plotted as the ratio of fluorescence in the absence of quencher (F_0) to the intensity in the presence of quencher (F) against quencher concentration. The resulting data were fit to dynamic parameters according to the Stern-Volmer equation (Lakowicz, 1983),

$$F_0/F = 1 + (K_{SV} \times [Q]), \quad (10)$$

where K_{SV} is the Stern-Volmer quenching constant and $[Q]$ the quencher concentration.

RESULTS AND DISCUSSION

Molecular model of adenylated *Ts*lig

The sequences of *T. scotoductus* (*Ts*lig) and *T. filiformis* (*Tf*lig) DNA ligases display 80% identity, allowing to build a model of the former (Fig. 1 *B*). All residues implicated in nick sensing and ligation activities in *Tf*lig (Lee et al., 2000) are conserved in *Ts*lig. Like the *Tf*lig template, *Ts*lig is a monomeric enzyme folded into four discrete domains (Fig. 1, *A* and *B*). Domain I (residues 1-320) consists of two subdomains, subdomain Ia, essentially α-helical (residues 1-73) and the ''adenylation'' domain (Ib), comprising two mainly antiparallel β-sheets flanked by α-helices and containing an adenylation site (residues 74-320). Domain 2 or ''OB fold domain'' contains a five-stranded antiparallel β-barrel (residues 321-406). Domain 3 consists of two subdomains, where subdomain 3a is a Cys_4-type zinc finger (residues 407-432) and subdomain 3b comprises four Helix-hairpin-Helix (HhH) motifs (residues 433-584). Domain 4 is a member of the BRCT (BRCA1 C-terminus) domain superfamily (residues 585-674). As shown for *Tf* DNA ligase (Lee et al., 2000), the circular arrangement of the four domains leads to a hole sufficiently large to hold a double-stranded DNA. In addition to 20 Phe (F) residues, *Ts*lig contains 21 Tyr (Y) residues and 6 Trp (W) residues, indicated in Fig. 1 *B*. Four tryptophanes, W135, W246, W274, and W298, are located within the active site, whereas W375 and W405 are located within the domain 2. W246 and W298 could make contact with AMP within the active site, whereas W135 is located too far and W274 is ''shielded'' by two β-sheets (Fig. 1 *B*). In addition, the adenine base of AMP is stacked against the side chain of Y226, which is conserved among all known NAD$^+$-dependent DNA ligases (Doherty and Suh, 2000; Lee et al., 2000). Finally, W135, W246, W274, and W405 are rather buried in the model, whereas W298 and W375 are relatively accessible to the solvent.

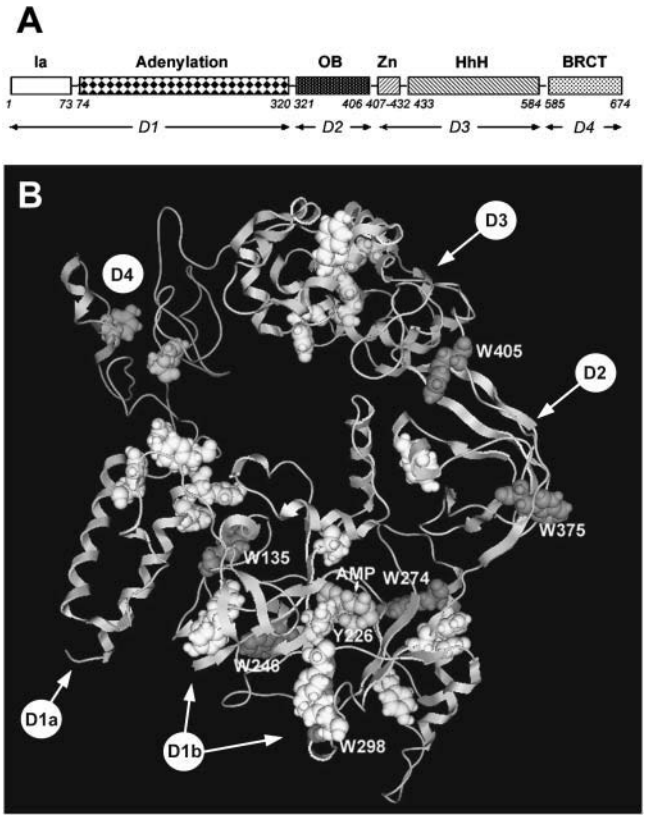

FIGURE 1 Domain structure of *T. scotodustus* DNA ligase. (*A*) *T. scotoductus* DNA ligase (*Ts*lig) is illustrated as a linear assortment of conserved structural domains (Ia, Adenylation, OB (Oligomer Binding) fold, Zn-binding, HhH (Helix-hairpin-Helix), and BRCT (BRCA1 C-terminus)). D1 to D4, domain 1 to domain 4. (*B*) Schematic view of the three-dimensional structure of *Ts*lig. The tryptophan (W) and tyrosine (Y) residues are rendered as white and gray space filled structures, respectively. *Ts*lig contains 6 W and 21 Y. The covalently bound AMP moiety is pointed out by an arrow.

Prediction of partially folded intermediates

Recently, it has been shown (Uversky, 2002a) that the competence of a protein to form equilibrium intermediate(s) I, may be determined by the bulk content of hydrophobic and charged amino acid residues. In fact, proteins unfolding through a N↔I$_{(x)}$↔U scheme are specifically localized within a unique region of a charge-hydrophobicity space, with $\langle H\rangle = 0.446 \pm 0.023$ and $\langle R\rangle = 0.027 \pm 0.022$, where $\langle H\rangle$ and $\langle R\rangle$ are the mean hydrophobicity and the mean net charge of the protein, respectively. The mean hydrophobicity $\langle H\rangle$ is defined as the sum of the normalized hydrophobicities of all residues divided by the number of residues in the polypeptide. The mean net charge $\langle R\rangle$ is defined as the net charge at pH 7.0, divided by the total number of residues. Analysis of the *Ts*lig amino acid sequence shows that this protein is characterized by $\langle H\rangle = 0.450$ and $\langle R\rangle = 0.007$, thus fulfilling the prediction for unfolding through intermediate states.

Effect of temperature on the structure of deadenylated and adenylated *Ts*lig

The thermal stabilities of deadenylated and adenylated *Ts*lig were compared by DSC. We have established that under conditions studied both forms unfold irreversibly, as demonstrated by the lack of ΔH_{cal} recovery during a second denaturation scan and by the dependence of calorimetric traces on scan rates (not shown). For each form, two distinct heat absorption peaks were observed (Fig. 2). The deconvolution of the excess heat capacity (C_p) functions revealed two and three subsequent transitions for deadenylated and adenylated *Ts*lig, respectively (Table 1). These results

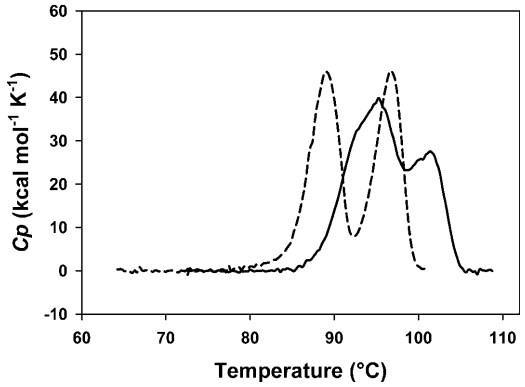

FIGURE 2 Thermal unfolding of *Ts*lig recorded by DSC. Adenylated *Ts*lig is characterized by higher T_{max} (top of the transition) and ΔH_{cal} (area under the transition). All thermograms are baseline-subtracted and normalized for protein concentrations. Deadenylated *Ts*lig (*dashed line*); adenylated *Ts*lig (*solid line*).

demonstrate that deadenylated and adenylated *Ts*lig denature according to a non-two-state mechanism. The deviation from a two-state model was further confirmed by the fact that $\Delta H_{cal}/\Delta H_{eff}$ ratio exceeds unity (not shown). Analysis of Table 1 also reveals that the adenylated enzyme displays an increase of ~5°C and 80 kJ mol^{-1} in the T_{max} and ΔH_{cal}, respectively. Such results clearly indicate that cofactor anchoring at the active site increases markedly the conformational stability of the enzyme.

Effect of GdmCl on the structure of deadenylated and adenylated *Ts*lig

Several spectroscopic techniques have been applied to study the GdmCl-induced unfolding of deadenylated and adenylated *Ts*lig. Unfolding of both forms was reversible because they regained native conformation following renaturation after complete denaturation in 7 M GdmCl (not shown).

TABLE 1 Thermodynamic parameters of heat-induced unfolding of deadenylated and adenylated *Ts*lig Parameters are determined from data shown in Fig. 2

	T_{max}* (°C)	Transitions (n)†	T_m‡ (°C)	ΔH_{cal} (kJ mol^{-1})	$\Sigma\ \Delta H_{cal}$ (kJ mol^{-1})
Deadenylated *Ts*lig	89.0	2	88.9	904	1649
	96.6		96.5	745	
Adenylated *Ts*lig	95.2	3	91.8	301	1729
	101.3		95.6	1009	
			101.4	417	

*T_{max} corresponds to the temperature at the top of the peak.
†n refers to the number of calorimetric domains identified by deconvolution of DSC thermograms.
‡T_m is the melting point of the unfolding transition.

Intrinsic fluorescence

The fluorescence emission spectra of the native forms of deadenylated and adenylated *Ts*lig (λ_{ex} 280 nm) show a single broad emission band with maxima at ~332 nm (Fig. 3, *A* and *B*, and Table 4). Excitation at 295 nm did not dramatically modify the shape of emission spectra (λ_{max} ~333 nm), except that the shoulder near 306 nm (contribution of the Tyr residues) disappeared (see Fig. 3, *A* and *B insets*). The λ_{max} values of native enzymes indicate that the Trp residues in both forms are relatively buried and that adenylation does not change significantly the net polarity of the Trp environment within the ''catalytic core'' of the protein (domain 1 and 2, see Fig. 1 *B*). However, adenylation quenched the fluorescence of *Ts*lig by ~35% (Fig. 3, *A* and *B*), demonstrating that cofactor binding induces at least conformational rearrangement within the active site. Quenching of fluorescence after cofactor binding has been reported for numerous enzymes (Brandes et al., 1998; Candy et al., 1996; Diefenbach and Duggleby, 1991; Favilla et al., 2002; Goenka et al., 2001; Gupta and Kang, 1997; Marchal and Branlant, 1999; Morimatsu et al., 1995; Murataliev and Feyereisen, 2000; Sinha et al., 1999; Tang et al., 2001). The observed quenching of intrinsic *Ts*lig

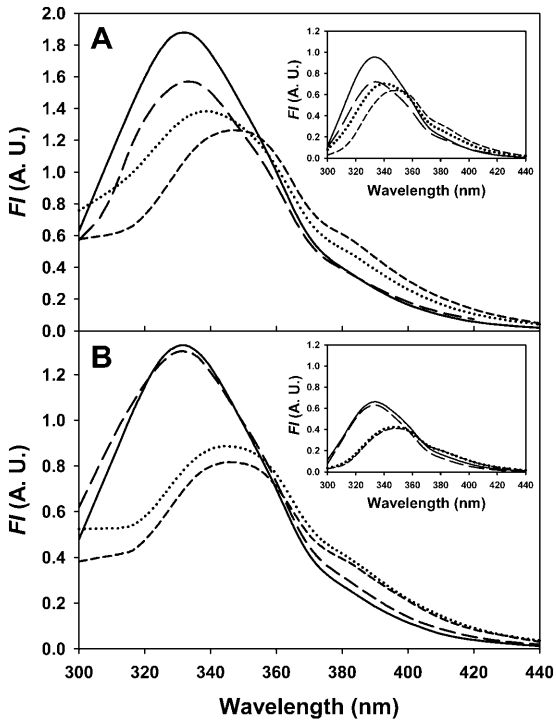

FIGURE 3 Fluorescence emission spectra of deadenylated and adenylated *Ts*lig. (*A*) Spectra of deadenylated *Ts*lig recorded on excitation at 280 nm at 0 M (*solid line*), 2.5 M (*long-dashed line*), 3.5 M (*dotted line*), and 6.5 M (*short-dashed line*) GdmCl. Inset represents spectra recorded on excitation at 295 nm. (*B*) Spectra of adenylated *Ts*lig recorded on excitation at 280 nm at 0 M (*solid line*), 3 M (*long-dashed line*), 4.4 M (*dotted line*), and 6.5 M (*short-dashed line*) GdmCl. Inset represents spectra recorded on excitation at 295 nm. Corresponding λ_{max} are given in Table 4.

fluorescence is likely due to an interaction of AMP with Y226 (the nucleotide is stacked against the side chain of Y226) and/or W246 and W298 (see also ''Molecular model of adenylated *Ts*lig''). In 6.5 M GdmCl, the wavelength of maximal emission is shifted to ~347 nm (λ_{ex} 280 nm) for both forms, indicating that they converge to an unfolded form exhibiting the same emissive properties with increased accessibility of the Trp residues to the bulk solvent (Fig. 3, *A* and *B*).

GdmCl-induced unfolding of deadenylated *Ts*lig monitored by the characteristic changes in fluorescence intensity (λ_{ex} 280 nm), FI_{333} and in *AEW* are consistent with a simple two-state model N↔U (Fig. 4, *A* and *B*). Satisfactory fits of the data could be obtained from Eq. 3, providing similar $\Delta G(H_2O)$, *m*, and *Cm* (concentration of GdmCl required for half-denaturation of the enzyme) values (Table 2).

Unlike the deadenylated form, GdmCl-induced unfolding of adenylated *Ts*lig monitored by FI_{333} (λ_{ex} 280 nm) supports a three-state unfolding model (N↔I↔U) in which a partially unfolded state (I) is significantly populated at intermediate GdmCl concentrations (~2–4 M) (Fig. 4 *A*). Fitting of the experimental data to Eq. 4 provides $\Delta G_{N\text{-}I}(H_2O)$ of 18.2 ± 3.4 kJ mol^{-1}, $\Delta G_{I\text{-}U}(H_2O)$ of 42.2 ± 4 kJ mol^{-1}, $Cm_{N\text{-}I}$ of 1.6 M and $Cm_{I\text{-}U}$ of 4.2 M (Table 2). Interestingly, the presence of this intermediate is not recorded by the *AEW* data (Fig. 4 *B*). In this case, unfolding occurs as a single transition, with a $\Delta G(H_2O)$ value of 38.8 ± 1.8 kJ mol^{-1} (which is significantly lower than the $\Sigma[\Delta G_{N\text{-}I}(H_2O) + \Delta G_{I\text{-}U}(H_2O)] = 60.4$ kJ mol^{-1}) and a *Cm* of 4.2 M (Table 2). Therefore, the N↔I transition can be attributed to the enzyme adenylation and describes the elimination of the AMP-induced quenching of the intrinsic fluorescence at 333 nm, which is not accompanied by a significant change of the environment of the tryptophan residues (λ_{max} is not red-shifted, see Fig. 3 *B*). In addition, comparison of the emission spectra (λ_{ex} 280 nm) of native enzyme with that of the enzyme in 3 M GdmCl (Fig. 3 *B*) reveals a change in the 300-nm region, attributed to the contribution of Tyr residues. The analysis of the *FI* at 306 nm as a function of GdmCl concentrations (Fig. 4 *C*) clearly demonstrates an increase of the fluorescence intensity at low and moderate GdmCl concentrations, with a maximum reached at ~2.5 M. One of the putative mechanisms responsible for this increase is a structural rearrangement of the protein, with a concomitant separation between one or some Tyr and Trp residue(s), leading to the suppression of the energy transfer from the former to the latter. Careful examination of Fig. 1 *B* reveals that some Tyr residues are located in the vicinity of the Trp residues, making such a hypothesis plausible. As a second possibility, AMP in the intermediate state, which was initially stacked against the side chain of Y226, could move away from this residue leading to a dequenching phenomenon and, thus to the observed increase in the tyrosine fluorescence emission. An interesting feature is that the AMP is not present in the deadenylated enzyme and that in this

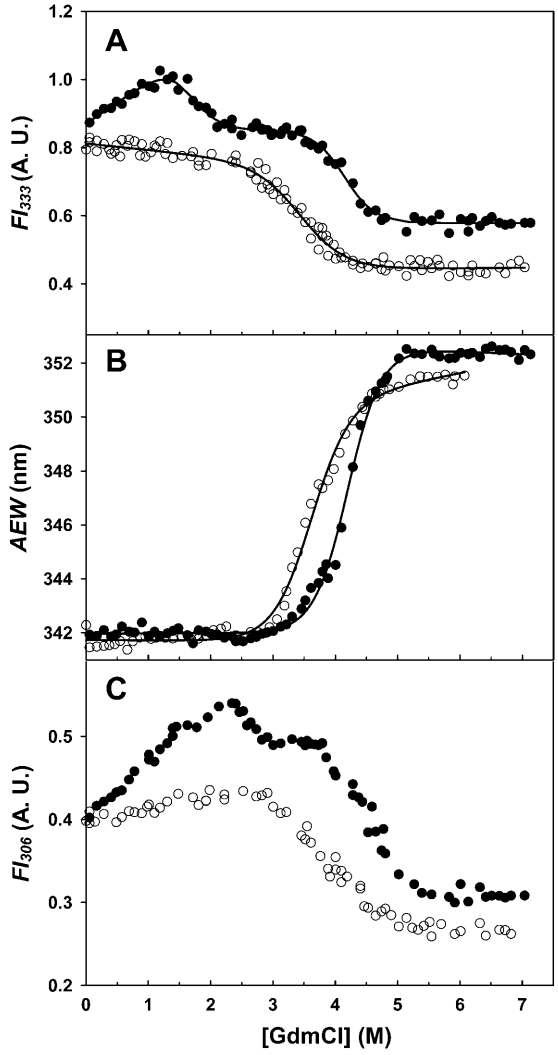

FIGURE 4 GdmCl-induced structural rearrangements of *Ts*lig, monitored by changes in fluorescence spectroscopy. Unfolding of (○) deadenylated and (●) adenylated *Ts*lig recorded by the changes of the fluorescence intensity (λ_{ex} 280 nm) at 333 nm (*A*), of the average emission wavelength (*B*), and of the fluorescence intensity (λ_{ex} 280 nm) at 306 nm (*C*). Data were analyzed according to a two-state reaction, except in *A* for adenylated *Ts*lig where a three-state pathway was used; the lines represent the best fits to Eqs. 3 (two states) and 4 (three states), calculated using the thermodynamic parameters in Table 2. A. U., arbitrary units. Measurements were carried out at pH 7.6, 25°C. Protein concentration was kept at 0.025 mg/ml.

form no significant fluorescence increase at 306 nm is noticed at low and moderate GdmCl concentrations (Fig. 4 *C*).

Finally, analysis of *m* values, as well as $\Delta G(H_2O)$ and *Cm* values estimated for apo- and holoforms emphasizes two important points. First, based on an expected theoretical *m* value of 60 kJ mol^{-1} (Myers et al., 1995), the low *m* values reported for deadenylated and adenylated *Ts*lig (Table 2) are likely to reflect deviation from a two-state mechanism (Myers et al., 1995; Pace, 1986). Second, comparison of $\Delta G(H_2O)$ and *Cm* values clearly indicates cofactor stabilization, as the adenylated enzyme shows a 9.9 kJ mol^{-1}

TABLE 2 Thermodynamic parameters* of GdmCl-induced unfolding of deadenylated and adenylated *Ts*lig, as obtained from the analysis of the equilibrium transitions

	$\Delta G(H_2O)$* (kJ mol^{-1})	m* (kJ mol^{-1})	C_m (M)	Transition monitored†
Deadenylated *Ts*lig				
Fluorescence (λ_{ex}^{280})				
FI (333 nm)	23.6 ± 2.5	6.8 ± 0.7	3.5	MG↔U
AEW	28.9 ± 2.0	8.0 ± 0.6	3.5	MG↔U
Adenylated *Ts*lig				
Fluorescence (λ_{ex}^{280})				
$FI_{N\text{-}I}$ (333 nm)	18.2 ± 3.4	11.2 ± 1.8	1.6	N↔MG
$FI_{I\text{-}U}$ (333 nm)	42.2 ± 4.0	10.2 ± 1.0	4.2	MG↔PMG
AEW	38.8 ± 1.8	9.3 ± 0.5	4.2	MG↔PMG
Circular dichroism				
near (280 nm)	12.3 ± 0.1	7.7 ± 0.1	1.6	N↔MG
near (260 nm)	31.2 ± 4.2	7.5 ± 1.1	4.2	MG↔PMG
$far_{N\text{-}I}$ (222 nm)	67.7 ± 12.7	19.0 ± 3.6	3.6	MG↔PMG
$far_{I\text{-}U}$ (222 nm)	27.4 ± 2.3	5.2 ± 0.4	5.2	PMG↔U

*All thermodynamic parameters were determined according to Eq. 3 (see Materials and Methods) except for fluorescence intensity and far-UV CD of adenylated *Ts*lig, in which thermodynamic parameters were calculated with the help of Eq. 4.

†N, native state; MG, molten globule state; PMG, premolten globule state, and U, unfolded state.

increase in the stabilization energy and a 0.7 M increase in *Cm* values (Table 2).

ANS fluorescence

Changes in ANS fluorescence are frequently used to detect accumulation of nonnative partially folded intermediates in globular proteins (Ptitsyn, 1995; Semisotnov et al., 1991). Such intermediates are characterized by the presence of solvent-exposed hydrophobic clusters, resulting in a pronounced blue shift of the fluorescence emission maximum (~525–480 nm) and a considerable enhancement of ANS fluorescence intensity at ~480 nm (Semisotnov et al., 1991). With native deadenylated and adenylated *Ts*lig, no binding of ANS could be observed. Fig. 5 shows that in the case of deadenylated *Ts*lig, an increase in GdmCl concentrations leads to considerable changes in the ANS fluorescence intensity at 480 nm, with the maximal fluorescence observed at 3.2 M GdmCl. This demonstrates that albeit the denaturation followed by changes in the intrinsic fluorescence can be described as a cooperative two-state process N↔U (Fig. 4, *A* and *B*), ANS binding experiments show that the chemical unfolding of the deadenylated enzyme is accompanied by accumulation of at least one intermediate with solvent-accessible nonpolar clusters. Unlike the deadenylated ligase, GdmCl-induced unfolding of adenylated *Ts*lig does not show any blue shift (not shown) and the ANS fluorescence at 480 nm is low and constant throughout the entire unfolding transition (Fig. 5), suggesting that no binding of the dye occurred. However, in this case, presence of AMP could cause alterations in the microenvironment of

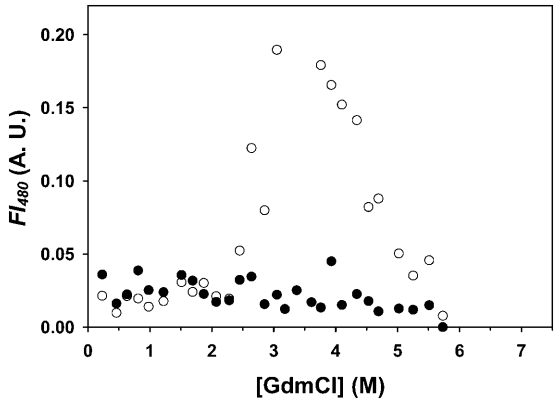

FIGURE 5 ANS fluorescence intensity. GdmCl dependence of ANS binding by *Ts*lig, measured by the intensity of ANS fluorescence at 480 nm (λ_{ex} 390 nm). (○) deadenylated and (●) adenylated *Ts*lig. A. U., arbitrary units. Measurements were carried out at pH 7.6, 25°C. Protein concentration was kept at 0.025 mg/ml.

the potential ANS binding site, preventing any binding between the intermediate state and the dye. In fact, displacement of ANS into a more polar environment upon cofactor binding has been already reported for various enzymes (D'Auria et al., 1999; Favilla et al., 2002; Kube et al., 1987; Shepherd and Hammes, 1976). Therefore, in adenylated *Ts*lig, it is likely that: i), the ANS binding site is at, or close to, the cofactor-binding site, i.e., the active site, and ii), the absence of ANS binding upon the whole unfolding transition is due to a steric constraint rather than to the absence of unfolding intermediates.

Circular dichroism

Further insights on the unfolding pathways of adenylated *Ts*lig were obtained by monitoring near- and far-UV CD spectra. It is worth mentioning that CD measurements were only performed for the adenylated form of *Ts*lig, because the remaining traces β-NMN in the deadenylated enzyme disturbed CD signal, preventing any accurate recording.

The near-UV CD spectrum of a protein reflects the asymmetric environment of its aromatic residues and thus probes the protein tertiary structure. Accordingly, denaturation is accompanied by the loss in intensity and fine structure of the near-UV CD signals. Fig. 6 *A* represents the near-UV spectra of adenylated *Ts*lig measured at different GdmCl concentrations. The native protein is characterized by a pronounced near-UV CD spectrum with a negative band in the 280-nm region due to the contribution of Tyr and Trp residues and an additional positive band around 260 nm, likely due to AMP contribution. The intensity of these bands decreased dramatically with the increase in GdmCl concentration, reflecting the denaturant-induced distortion of rigid tertiary structure. The change in $[\theta]_{260}$ (Fig. 6 *B*, *top panel*) and $[\theta]_{280}$ (Fig. 6 *B*, *bottom panel*) show that the GdmCl-

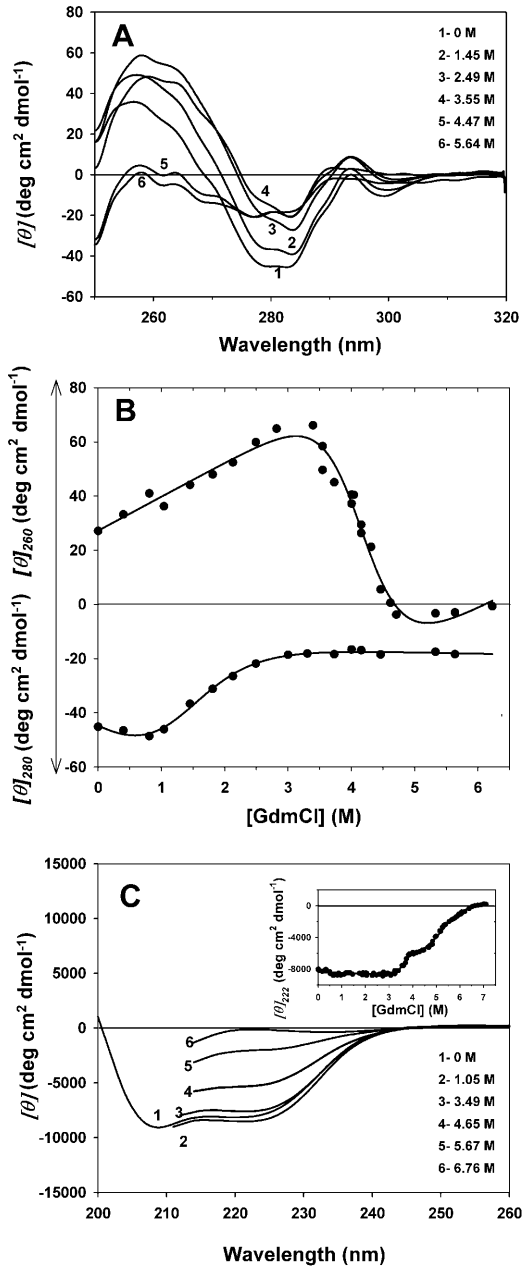

FIGURE 6 GdmCl-induced unfolding transitions of adenylated *Ts*lig followed by near/far UV CD changes. (*A*) CD spectra (smoothed data) in the near UV region of *Ts*lig. (*B*) Equilibrium unfolding transitions of *Ts*lig followed by near-UV CD measurements at 260 nm (*top panel*) and at 280 nm (*bottom panel*). (*C*) CD spectra (smoothed data) in the far UV region of *Ts*lig; inset represents equilibrium unfolding transitions followed by CD measurements at 222 nm. Data were analyzed on the basis of a two-state (Eq. 3) and three-state model (Eq. 4) for near- and far-UV CD, respectively; the lines represent the best fits, calculated using the thermodynamic parameters in Table 2. Measurements were carried out at pH 7.6, 25°C. In the near UV, protein concentration was 1 mg/ml in a 1-cm cell. In the far UV, protein concentration was 0.25 mg/ml in a 0.1-cm cell.

induced denaturation of protein is described by a simple sigmoidal curve, consistent with a two-state transition. Interestingly, *Cm* calculated for the $[\theta]_{260}$ vs. [GdmCl] dependence is 4.2 M (Table 2), which corresponds to the *Cm* of the second transition detected by changes in intrinsic fluorescence ($Cm_{\text{I-U}}$). On the other hand, the calculated *Cm* for the transition monitored by changes at 280 nm is 1.6 M (Table 2), which is in a good agreement with *Cm* of the first transition detected by changes in the fluorescence intensity ($Cm_{\text{N-I}}$). These discrepancies between the CD denaturation profiles at 260 and 280 nm clearly demonstrate that the loss of the tertiary structure does not occur according to a simple N↔U model, but follows a more complex pathway involving at least one intermediate state.

The far-UV spectra of adenylated *Ts*lig (Fig. 6 *C*) were also used to analyze the conformation of its polypeptide backbone. The native form exhibits double minima at 208 nm and 222 nm, typical of proteins containing α-helical secondary structures. Based on Eq. 2, its α-helical content was estimated to be ~19%. The GdmCl-resistance of the enzyme was also investigated by far-UV CD measurements (Fig. 6 *C*). At low GdmCl concentrations, a slight decrease of the ellipticity is observed, which maintains until ~3 M GdmCl. This decrease could be attributed to: i), a stabilization effect of GdmCl because it is known that NAD$^+$-dependent DNA ligases are stabilized by salt or ii), to the formation of an intermediate state such as a molten globule (MG). The second hypothesis is supported by the fact that MG with far-UV spectra more pronounced than those of native proteins have been observed in a number of proteins (for review, see Vassilenko and Uversky (2002)). No significant changes in far-UV CD spectra is noticed up to 3.5 M GdmCl, pointing out that the formation of the intermediate state (*Cm* 1.6 M), detected by fluorescence and near-UV (280 nm) studies, is not accompanied by noticeable changes in protein secondary structure. In addition, the analysis of the GdmCl dependence of ellipticity at 222 nm (Fig. 6 *C*, *inset*) reveals that adenylated *Ts*lig unfolding can be described by two successive sigmoidal curves, separated by a short plateau around 4 M GdmCl. The *Cm* of the first transition is 3.6 M (Table 2) whereas that of the second transition is 5.15 M, which is higher than that observed with the fluorescence intensity ($Cm_{\text{I-U}}$ of 4.2 M). Finally, the calculated α-helical content at 1.6 M, 3.6 M, 4.2 M, and 5.1 M GdmCl was shown to be ~19%, 17.3%, 11.5%, and 2.8%, respectively. All these results point out that adenylated *Ts*lig unfolds through at least two intermediates. The first intermediate is characterized by a loosely packed protein core and native-like content of secondary structure, i.e., it has properties similar to those of the molten globule state (Ptitsyn, 1995). As for the second intermediate, it is less compact and less structured than the first one but still much more compact and more structured than the fully unfolded protein, displaying properties of the premolten globule state (Ptitsyn, 1995). We must emphasize here that this state is no longer considered as a ''folding exception'' because it has been reported for many enzymes (for review, see Uversky and Fink (2002)).

"Phase diagram" analysis of circular dichroism data

Representation of CD data in a form of ''phase diagrams'' (see Materials and Methods) provided an additional support to the idea that GdmCl-induced unfolding of adenylated *Ts*lig is an exceptionally complex process. Application of this method to protein unfolding predicts that the dependence of $I_{(\lambda 1)} = f(I_{(\lambda 2)})$ will be linear if changes in the protein environment lead to all-or-none transition between two different conformations. On the other hand, nonlinearity of this function reflects the sequential character of structural transformations. Moreover, each linear portion of the $I_{(\lambda 1)} = f(I_{(\lambda 2)})$ dependence will describe an individual all-or-none transition.

Fig. 7 illustrates the phase diagrams for the GdmCl unfolding of adenylated *Ts*lig based on the analysis of near- and far-UV CD. In the near-UV CD (Fig. 7 *A*), the phase diagram consists of three linear parts, reflecting the existence of at least three independent transitions separating four different conformational states, i.e., N, an additional intermediate N* in the range of 0–1.0 M GdmCl, MGsw (swollen MG), and U. In the case of the analysis based on far-UV CD (Fig. 7 *B*), the phase diagram consists of four linear parts, reflecting the existence of five different conformational states, i.e., N, N*, MG, premolten globule (PMG) (see ''Size exclusion chromatography'' section), and U. Finally, all conformational states occurring upon unfolding were highlighted when the analysis was based on the comparison of near- and far-UV CD. The appearance of the N* intermediate (Fig. 7) could be due to a salt effect of GdmCl on structure of adenylated *Ts*lig, as previously mentioned (see ''Circular dichroism'' section). Compaction of the native conformation and/or enhanced stability of the protein due to Gdm^+ binding to negatively charged moieties of protein has been reported for multimeric (Akhtar et al., 2002) as well monomeric (Mayr and Schmid, 1993) proteins.

Analysis of unfolding intermediates by size exclusion chromatography

To obtain information about the effect of GdmCl on the hydrodynamic dimensions of deadenylated and adenylated *Ts*lig and their unfolding intermediates, the gel-filtration behavior of the proteins under different experimental conditions was studied. SEC separates proteins by differences in their hydrodynamic dimensions rather than by their molecular masses (Ackers, 1970). This approach has been successfully applied to determine the Stokes radius (R_S) values for proteins in different conformational states (Uversky, 1993; Uversky and Ptitsyn, 1994, 1996). Fig. 8 presents FPLC profiles of deadenylated (*A*) and adenylated (*B*) *Ts*lig (at 25°C) in solutions with different concentrations of GdmCl.

Native deadenylated *Ts*lig elutes as a single peak, whose elution volume corresponds to a protein with a R_S of 32.5 Å

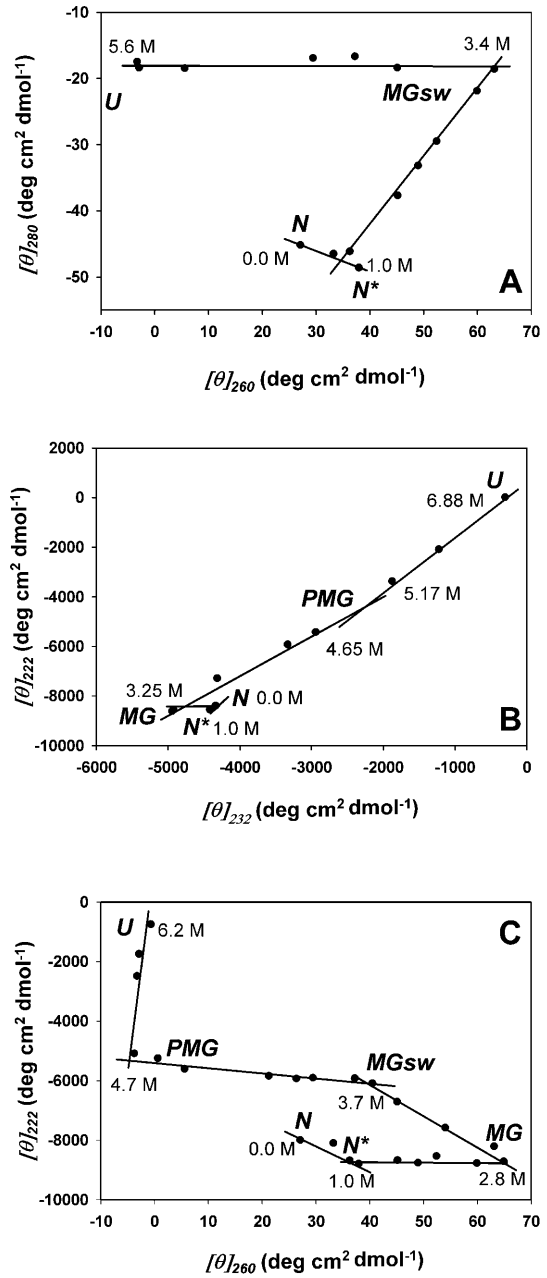

FIGURE 7 Phase diagram based on near- and far-UV CD spectra of adenylated *Ts*lig and representing the enzyme unfolding induced by an increase in GdmCl concentration. Denaturant concentration values are indicated in the vicinity of the corresponding symbol. Each straight line represents an all-or-one transition between two conformers. (*A*) Phase diagram based on near-UV CD ($[\theta]_{280}$ vs. $[\theta]_{260}$); (*B*) phase diagram based on far-UV CD ($[\theta]_{222}$ vs. $[\theta]_{232}$); (*C*) phase diagram based on near/far-UV CD ($[\theta]_{222}$ vs. $[\theta]_{260}$).

(Table 3). This value is in excellent agreement with the R_S calculated for a native globular protein with a molecular mass of 76.5 kDa (Table 3) (Uversky, 2002b). When the GdmCl concentration increases, the peak is substantially shifted to smaller elution volumes, corresponding to the transition to a slightly more expanded compact denatured state (molten

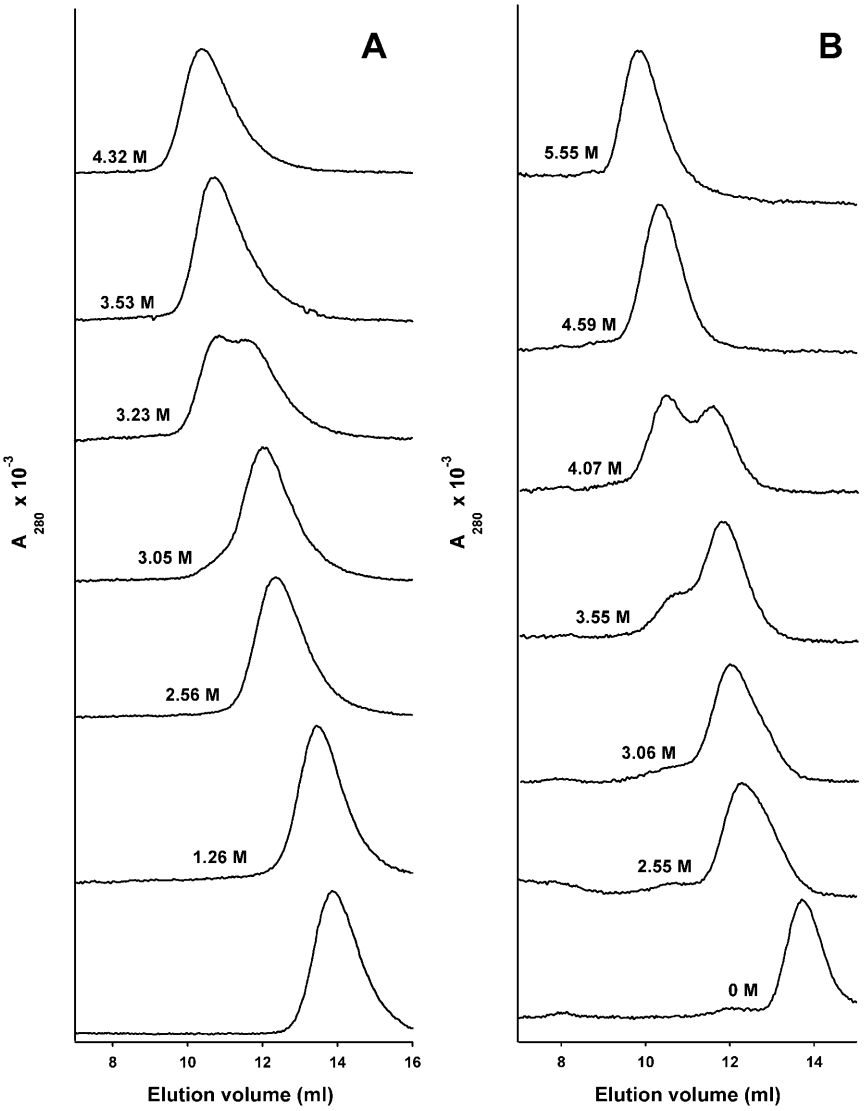

FIGURE 8 Elution profiles of *Ts*lig on size-exclusion chromotography. Deadenylated (*A*) and adenylated (*B*) *Ts*lig (0.25 mg/ml) were loaded on a Superdex 200 H/R column at 25°C in 20 mM sodium phosphate buffer, 250 mM NaCl, pH 7.6, at different GdmCl concentrations.

globules) and the swelling of the MG state (MG_{sw}) (Figs. 8 *A* and 9 *A*). In the vicinity of 3–3.5 M GdmCl, the appearance of a separate peak indicates the transformation of the MG into a less compact state (LC) (Figs. 8 *A* and 9 *A*). In addition, as shown on Fig. 9 *A*, the elution volume of the LC state strongly depends on the GdmCl concentration, and this dependence is much stronger than that for the unfolded molecules (LC approaches its baseline only at ~4 M

TABLE 3 Molecular dimensions of deadenylated and adenylated *Ts*lig in different conformational states

	Deadenylated *Ts*lig					Adenylated *Ts*lig				
State	GdmCl (M)	V^{el} (ml)	R_S, exp* (Å)	R_S, theo† (Å)	$R_S/(R_S)_N$	GdmCl (M)	V^{el} (ml)	R_S, exp* (Å)	R_S, theo‡ (Å)	$R_S/(R_S)_N$
Native (N)	0	13.88	32.5	34.6	1.00	0	13.72	33.4	34.7	1.00
Molten globule (MG)‡	2.50	12.44	41.6	37.9	1.28	3.06	12.01	44.8	37.9	1.32
Pre-molten globule (LC_{max}) (PMG)	3.04	11.20	51.4	50.6	1.58	3.06	10.99	53.3	50.7	1.60
Unfolded (U)	4.32	10.40	58.9	84.9	1.81	6.30	9.50	68.9	85.1	2.06

*R_S values calculated using the experimental equation $R_S = (1000/V^{el} - 42.44)/0.9114$.

†R_S values calculated using the equations described in Uversky (2002b): for N state, $\log(R_S) = -0.204 + 0.357 \log (M)$; for MG state, $\log(R_S) = -0.053 + 0.334 \log (M)$; for PMG state, $\log(R_S) = -0.21 + 0.392 \log (M)$, and for U state, $\log(R_S) = -0.723 + 0.543 \log (M)$.

‡Maximum population of MG (see also Fig. 9, *E* and *F*).

GdmCl). Concerning the native adenylated *Ts*lig, it also elutes as a single peak (Fig. 8 *B*), whose elution volume corresponds to a protein with R_S of 33.4 Å (Table 3). In the presence of denaturant, the elution profiles of the adenylated enzyme (Figs. 8 *B* and 9 *B*) display the same trends as that of the deadenylated protein, except that changes in elution profile occur at higher GdmCl concentrations, reflecting cofactor-induced stabilization of the enzyme.

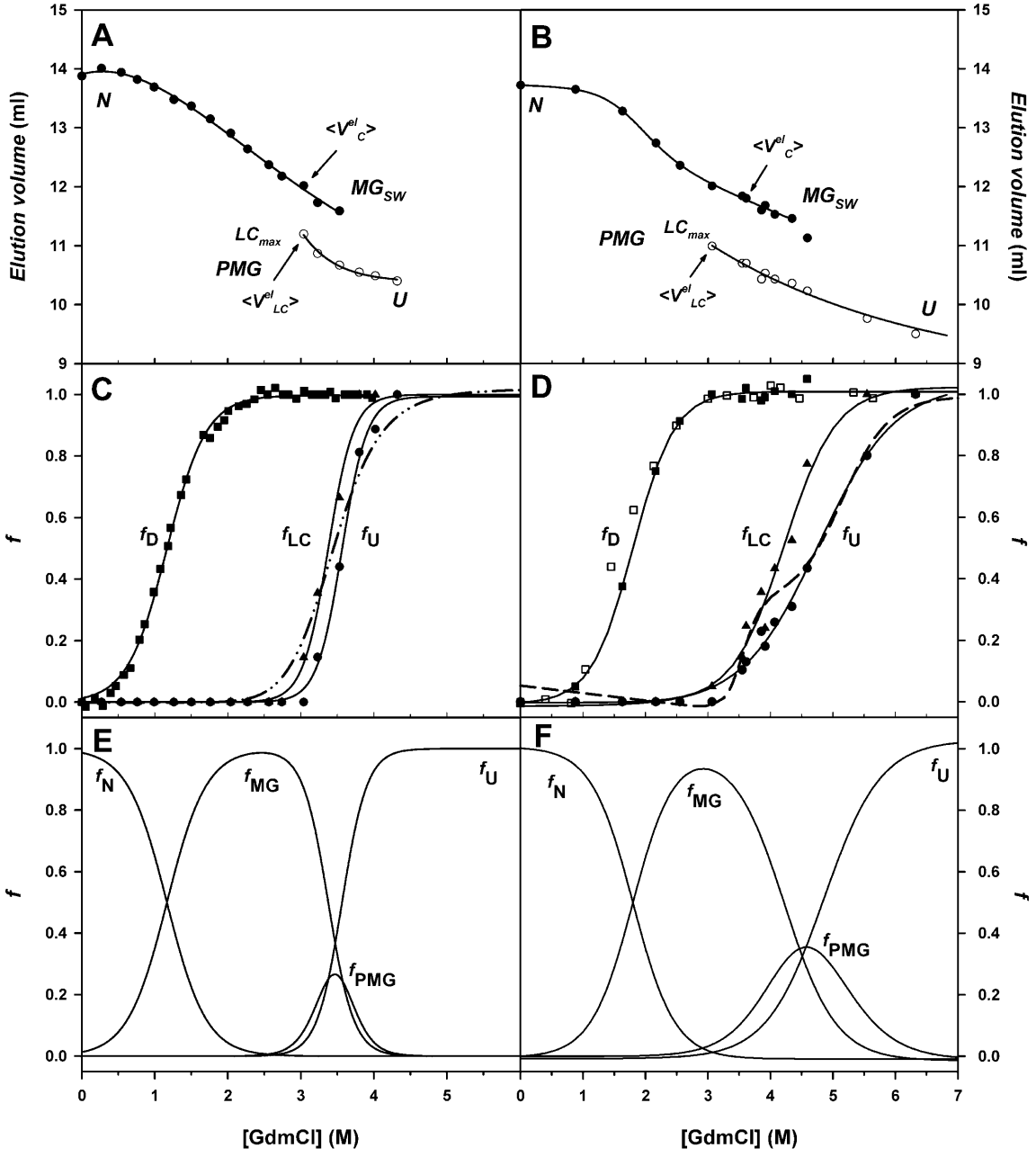

FIGURE 9 GdmCl-induced unfolding transitions of *Ts*lig monitored by size-exclusion chromatography. Dependence of elution volumes V^{el} of deadenylated (*A*) and adenylated (*B*) *Ts*lig on GdmCl concentrations. $\langle V_C \rangle$, elution volumes of ''compact'' molecules and $\langle V_{LC}{}^{el} \rangle$, elution volumes of ''compact'' molecules and $\langle V_{LC} \rangle$, elution volumes of ''less compact'' molecules $\langle V_{LC}{}^{el} \rangle$, elution volumes of ''less compact'' molecules. LC_{max}, maximal value of V^{el} for less compact molecules. N, native state; MG_{SW}, swollen molten globule state; PMG, premolten globule state; U, unfolded state. Stages of unfolding (four-state transition) of deadenylated (*C*) and adenylated (*D*) *Ts*lig. (*C*) Fraction of denatured molecules f_D was obtained from the relative change of elution volumes from 0 to 3.53 M GdmCl (N↔MG transition) (■); f_{LC}, fraction of less compact molecules (▲); f_U, fraction of unfolded molecules (●); fluorescence average emission wavelength, (*dash-dotted line*). (*D*) Fraction of denatured molecules f_D obtained from the relative change of near UV ellipticity $[\theta]_{280}$ (□) and the relative change of elution volumes from 0 to 4.34 M GdmCl (N↔MG transition) (■); f_{LC}, (▲); f_U, (●); relative change of far UV ellipticity $[\theta]_{222}$ (*dashed line*). Multiple-state GdmCl-induced N↔U transition in deadenylated (*E*) and adenylated (*F*) *Ts*lig presented in terms of fractions of different states: f_N, fraction of molecules in the native state; f_{MG}, fraction in the molten-globule state; f_{PMG}, fraction in the premolten globule state, and f_U, fraction in the unfolded state.

Fig. 9, *C* and *D*, also demonstrates the existence of three different stages in GdmCl-induced unfolding of deadenylated and adenylated *Ts*lig. The first stage (f_D) reflects protein denaturation, whereas two others stages (f_{LC} and f_U) correspond to two conformational transitions of an already-denatured protein. Three stages of unfolding correspond to the formation of at least two intermediates between the native and unfolded states, i.e., it is a four-state process. The first intermediate displays all the properties of the molten globule. It is almost as compact as the native protein, with a ~30% R_S increase (Table 3). Such increase is quite high compared to the usual 15–20% increase of R_S associated with MG formation (Ptitsyn, 1995; Uversky, 1993): for both forms the expected R_S is 37.9 Å (Table 3). Importantly, Fig. 9, *C* and *D*, show that the hydrodynamic dimensions of MG *Ts*lig (in particular that of the adenylated form) increase with the increase in denaturant concentration; i.e., the molten globule swells considerably. For the adenylated enzyme, extrapolation of the plateau after the N→MG transition to 0 M GdmCl gives an elution volume corresponding to a R_S of nonswollen MG, 36.2 Å. Thus, the actual increase in R_S is ~9%, which coincides with the usually observed increase of R_S associated with the MG formation. The first intermediate is also characterized by the lack of rigid tertiary structure but possesses a pronounced secondary structure, as demonstrated by near- and far-UV CD spectra for adenylated *Ts*lig in Fig. 6. Finally, in the presence of moderate concentrations of GdmCl the deadenylated enzyme is able to bind ANS (see above), reflecting an increased solvent accessibility of hydrophobic patches on the surface of the protein.

The second intermediate possesses all the properties of the PMG state. It is less compact than the molten globule but much more compact than the unfolded state (Table 3). In addition, the experimental R_S (51.4 Å and 53.3 Å for dea- and adenylated *Ts*lig, respectively) are in agreement with the theoretical R_S for PMG (50.7 Å for both forms). It also still contains substantial secondary structure, as demonstrated by far-UV CD spectra for adenylated *Ts*lig (Fig. 9 *D*). Analysis of f_{LC} and f_U of deadenylated and adenylated *Ts*lig (Fig. 9, *C* and *D*) points out that in the case of the deadenylated enzyme the LC→U transformation occurs in a narrower range of denaturant concentrations, assessing that cofactor stabilization affects all stages of unfolding.

Finally, at high GdmCl concentrations, both forms are considerably unfolded and characterized by R_S of 58.9 and 68.9 Å for deadenylated and adenylated enzyme, respectively (Table 3). Those values are however lower than the expected R_S values, i.e., 84.9 Å and 85.1 Å for deadenylated and adenylated *Ts*lig, respectively.

The four-state N↔U transition can be visualized by plotting the fractions of molecules in all four states (N, MG, PMG, and U) as a function of GdmCl concentrations (Fig. 9, *E* and *F*). The plots illustrate that the molten globule state appears at the first step of unfolding at the expense of the native state and that it transforms first into the premolten globule and then into the unfolded state. The maximum of population of the MG state corresponds to 2.5 M GdmCl for deadenylated *Ts*lig and 3.1 M GdmCl for adenylated *Ts*lig, whereas the maximum of population of the PMG state corresponds to 3.5 M GdmCl for deadenylated *Ts*lig and 4.4 M GdmCl for adenylated *Ts*lig. For the deadenylated enzyme, the U is reached at ~4 M denaturant although it is only reached at ~6 M for the adenylated ligase. All together, these results nicely illustrate that AMP binding leads to conformational changes protecting the enzyme against denaturation.

Fluorescence quenching

To gain additional information on the structural changes associated with cofactor binding and on the different folding intermediates accumulated during unfolding, a dynamic quenching investigation was performed on both preparations, using acrylamide as a quencher. Due to its polar nature, this molecule quenches the surface-exposed and partially buried Trp residues. A rigorous approach to probe Trp accessibility in the different conformers usually requires determination of the bimolecular rate constant kq ($kq = K_{SV}\ \tau_0$, where K_{SV} is the Stern-Volmer constant and τ_0 the fluorescence lifetime). However *Ts*lig contains 6 Trp therefore impairing the determination of individual τ_0. As generally accepted in such cases, conformational changes were investigated by comparing K_{SV} constants rather than kq constants. Fig. 10 represents the Stern-Volmer plots for deadenylated (Fig. 10 *A*) and adenylated (Fig. 10 *B*) *Ts*lig, under different experimental conditions and Table 4 shows the K_{SV} of the fitted curves. Analysis of K_{SV} of native deadenylated ($7.11 \pm 0.11\ M^{-1}$) and adenylated ($5.66 \pm 0.05\ M^{-1}$) enzymes clearly demonstrates a greater solvent accessibility for deadenylated *Ts*lig. Based on the structure of the *Tf* DNA ligase, the adoption of an open form in the deadenylated state and a closed form in the adenylated state has been suggested (Cherepanov and de Vries, 2002; Lee et al., 2000). Our results provide a direct evidence for the occurrence of an open-closure mechanism of the NAD$^+$-DNA ligase upon adenylation, as tryptophanes in the closed form are less accessible to the quencher, leading to a decreased K_{SV} value.

Quenching of folding intermediates was also investigated and revealed that the adenylation state influences the sensitivity of the protein to the quencher. For the deadenylated enzyme, the MG state (2.5 M GdmCl) displays almost the same K_{SV} as the native enzyme. Furthermore, examination of the fluorescence emission maximum, λ_{max}^{295} (Fig. 3 *A*) does not reveal any significant change in the exposure of Trp residues to the solvent. Upon PMG formation (3.5 M GdmCl), the accessibility of Trps to the quenching agent and solvent increases rendered by a higher K_{SV} and a red shift of the λ_{max}^{295} (~6 nm, see Fig. 3 *A* and

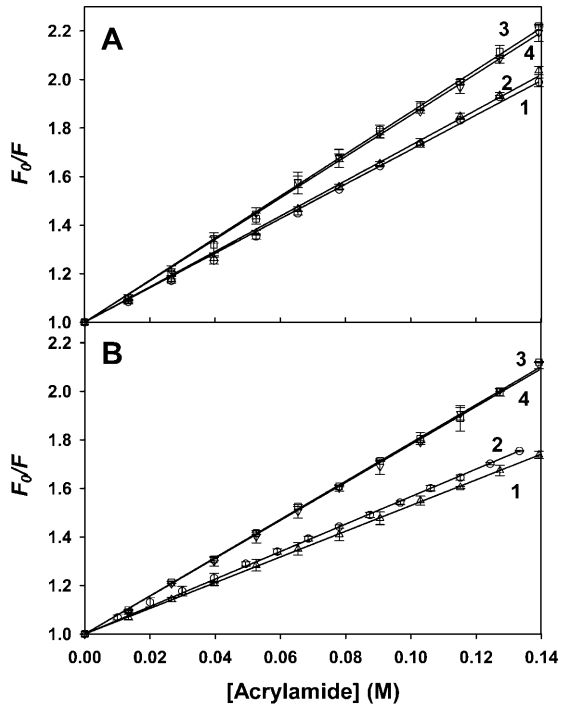

FIGURE 10 Trp fluorescence quenching by acrylamide. Quenching experiments of deadenylated (*A*) and adenylated (*B*) *Ts*lig were conducted as described under ''Experimental Procedures.'' (*A*) Fluorescence intensity of deadenylated *Ts*lig (λ_{ex} 295 nm, λ_{em} 333 nm) at 0 M (1), 2.5 M (2), 3.5 M (3), and 6.5 M GdmCl (4). (*B*) Fluorescence intensity of adenylated *Ts*lig recorded at 0 M (1), 3.06 M (2), 4.4 M (3), and 6.5 M (4) GdmCl. The quenching constant K_{SV} values corresponding to the plot slope (Eq. 10) are given in Table 4.

Table 4). Finally, the K_{SV} of the U state (6.5 M GdmCl) was close to that of the PMG, whereas the λ_{max}^{295} still increased (350 nm), reflecting the full exposure of Trp residues at high denaturant concentrations. Interestingly, the MG state of the adenylated enzyme (3.06 M GdmCl) shows a slightly decreased K_{SV} compared to the native protein (Fig. 10 *B*). The main cause for this result cannot be explained by a significant burial of the Trp residues in a hydrophobic environment because no major blue shift of the fluorescence emission maximum, λ_{max}^{295} was observed (Fig. 3 *B* and Table 4). In contrast, the PMG state of the adenylated *Ts*lig (4.4 M GdmCl) is characterized by an increased K_{SV} compared to the deadenylated enzyme and comparable to that of the unfolded state (Table 4). These results suggest that Trp residues in those forms are substantially solvated and accessible to the quencher molecules. This conclusion was further confirmed by the analysis of the position of maximal fluorescence, λ_{max}^{295} (Fig. 3 *B* and Table 4), which demonstrates concomitant changes in the exposure of Trps to solvent. Thus, the results of quenching experiments indicate that the Trp residues in the MG states of apo- and holoenzymes are in the same global environment as those of the native enzyme. On the other hand, in the PMG state Trp residues are significantly exposed to the solvent, suggesting more pronounced conformational changes than in the case of the MG.

TABLE 4 Stern-Volmer quenching constants (K_{SV}) and λ_{max} (nm) obtained for deadenylated and adenylated *Ts*lig under different GdmCl concentrations

GdmCl (M)	Deadenylated *Ts*lig			Adenylated *Ts*lig		
	K_{SV} (M^{-1})*	†λ_{max}^{280}	‡λ_{max}^{295}	K_{SV} (M^{-1})*	†λ_{max}^{280}	‡λ_{max}^{295}
0	7.11 ± 0.11	332.2	333.0	5.66 ± 0.05	332.0	333.6
2.5	7.28 ± 0.10	333.6	333.6			
3.0				5.29 ± 0.02	332.0	332.9
3.5	8.66 ± 0.12	338.2	339.9			
4.4				7.87 ± 0.07	344.0	348.3
6.5	8.53 ± 0.08	347.0	350.0	7.81 ± 0.08	346.0	350.0

*The Stern-Volmer quenching constants were obtained from the slopes of the lines for the plots of $F_0/F = 1 + (K_{SV} \times [Q])$.
†The excitation wavelength was 280 nm.
‡The excitation wavelength was 295nm.

CONCLUSION

In this report, we provide new insights into the conformational changes occurring upon adenylation of NAD^+-dependent DNA ligases. Although previous works had suggested such changes (Cherepanov and de Vries, 2002; Doherty and Suh, 2000; Lee et al., 2000), our biophysical analyses on the deadenylated and adenylated *Ts*lig firmly demonstrate that the transformation of the cofactor-free enzyme into its catalytically active form causes a conformational rearrangement within its active site accompanied by the compaction of the enzyme. These results support an ''open-closure'' induced-mechanism avoiding the formation of nonproductive ligase-DNA complexes. Mutational studies performed on aromatic residues located within the active site will be instrumental in the identification of the amino acid(s) involved in the conformational changes associated with adenylation.

The structural modifications occurring upon adenylation have also profound effects on the conformational stability of the enzyme. Upon adenylation, the conformational stability of the DNA ligase significantly increases, as demonstrated by differential scanning microcalorimetry and guanidine hydrochloride denaturation. Cofactor molecules have long been known to stabilize enzymes specifically by stabilizing their active site. Our results obviously indicate that this observation is also valid for *Ts*lig, establishing a thermodynamic link between cofactor binding and conformational stability. Furthermore, the effect of DNA binding on the conformational stability of the enzyme is expected to give supplementary information on the substrate-induced modulation of enzyme stability.

To gain information about the deadenylated and adenylated conformers, the unfolding pathways of deadenylated and adenylated *Ts*lig have been followed by a combination of different biophysical methods. The GdmCl-induced equi-

librium unfolding of both forms can be described by a four-state transition model, N↔MG↔PMG↔U, shifted toward higher GdmCl concentrations in the case of adenylated enzyme.

We thank N. Gérardin and R. Marchand for their skillful technical assistance. We also thank F. Biemar, C. Houssier, A. Matagne, A. R. Merrill, and M. Vanhove for helpful assistance and discussions.

This work was supported by the European Union (Grant CT970131), the Région Wallonne (Grants Bioval 981/3860, Bioval 981/3848, Initiative 114705), the Fonds National de la Recherche Scientifique Belgium (Grant 2.4515.00), and the Institut Polaire Français. The purchase of the Jasco 810 equipment was supported in part by a grant from the Fonds de la Recherche Fondamentale et Collective (contract 2.4545.01).

REFERENCES

Ackers, G. K. 1970. Analytical gel chromatography of proteins. *Adv. Protein Chem.* 24:343–446.

Akhtar, M. S., A. Ahmad, and V. Bhakuni. 2002. Guanidinium chloride- and urea-induced unfolding of the dimeric enzyme glucose oxidase. *Biochemistry.* 41:3819–3827.

Aravind, L., and E. V. Koonin. 1999. Gleaning non-trivial structural, functional and evolutionary information about proteins by iterative database searches. *J. Mol. Biol.* 287:1023–1040.

Barany, F., and D. H. Gelfand. 1991. Cloning, overexpression and nucleotide sequence of a thermostable DNA ligase-encoding gene. *Gene.* 109:1–11.

Chen, Y. H., J. T. Yang, and H. M. Martinez. 1972. Determination of the secondary structures of proteins by circular dichroism and optical rotatory dispersion. *Biochemistry.* 11:4120–4131.

Brandes, H. K., F. W. Larimer, T. Y. Lu, J. Dey, and F. C. Hartman. 1998. Roles and microenvironments of tryptophanyl residues of spinach phosphoribulokinase. *Arch. Biochem. Biophys.* 352:130–136.

Brannigan, J. A., S. R. Ashford, A. J. Doherty, D. J. Timson, and D. B. Wigley. 1999. Nucleotide sequence, heterologous expression and novel purification of DNA ligase from *Bacillus stearothermophilus*[1]. *Biochim. Biophys. Acta.* 1432:413–418.

Burstein, E. A. 1976. Intrinsic Protein Fluorescence: Origin and Applications. Series Biophysics, Vol. 7, Viniiti, Moscow .

Bushmarina, N. A., I. M. Kuznetsova, A. G. Biktashev, K. K. Turoverov, and V. N. Uversky. 2001. Partially folded conformations in the folding pathway of bovine carbonic anhydrase II: a fluorescence spectroscopic analysis. *Chembiochem.* 2:813–821.

Candy, J. M., J. Koga, P. F. Nixon, and R. G. Duggleby. 1996. The role of residues glutamate-50 and phenylalanine-496 in *Zymomonas mobilis* pyruvate decarboxylase. *Biochem. J.* 315:745–751.

Cherepanov, A. V., and S. de Vries. 2002. Dynamic mechanism of nick recognition by DNA ligase. *Eur. J. Biochem.* 269:5993–5999.

D'Auria, S., P. Herman, M. Rossi, and J. R. Lakowicz. 1999. The fluorescence emission of the apo-glucose oxidase from *Aspergillus niger* as probe to estimate glucose concentrations. *Biochem. Biophys. Res. Commun.* 263:550–553.

Depiereux, E., G. Baudoux, P. Briffeuil, I. Reginster, X. De Bolle, C. Vinals, and E. Feytmans. 1997. Match-Box_server: a multiple sequence alignment tool placing emphasis on reliability. *Comput. Appl. Biosci.* 13:249–256.

Diefenbach, R. J., and R. G. Duggleby. 1991. Pyruvate decarboxylase from *Zymomonas mobilis*. Structure and re-activation of apoenzyme by the cofactors thiamin diphosphate and magnesium ion. *Biochem. J.* 276: 439–445.

Doherty, A. J., and T. R. Dafforn. 2000. Nick recognition by DNA ligases. *J. Mol. Biol.* 296:43–56.

Doherty, A. J., and S. W. Suh. 2000. Structural and mechanistic conservation in DNA ligases. *Nucleic Acids Res.* 28:4051–4058.

Favilla, R., M. Goldoni, A. Mazzini, P. Di Muro, B. Salvato, and M. Beltramini. 2002. Guanidinium chloride induced unfolding of a hemocyanin subunit from *Carcinus aestuarii*. I. Apo form. *Biochim. Biophys. Acta.* 1597:42–50.

Fechteler, T., U. Dengler, and D. Schomburg. 1995. Prediction of protein three-dimensional structures in insertion and deletion regions: a procedure for searching data bases of representative protein fragments using geometric scoring criteria. *J. Mol. Biol.* 253:114–131.

Georlette, D., Z. O. Jonsson, F. Van Petegem, J. Chessa, J. Van Beeumen, U. Hubscher, and C. Gerday. 2000. A DNA ligase from the psychrophile *Pseudoalteromonas haloplanktis* gives insights into the adaptation of proteins to low temperatures. *Eur. J. Biochem.* 267:3502–3512.

Goenka, S., B. Raman, T. Ramakrishna, and C. M. Rao. 2001. Unfolding and refolding of a quinone oxidoreductase: α-crystallin, a molecular chaperone, assists its reactivation. *Biochem. J.* 359:547–556.

Goldberg, M. E., N. Expert-Bezançon, L. Vuillard, and T. Rabilloud. 1995. Non-detergent sulphobetaines: a new class of molecules that facilitate *in vitro* protein renaturation. *Fold. Des.* 1:21–27.

Gupta, G. S., and B. P. Kang. 1997. LDH-C4-substrate binary complexes studied by intrinsic fluorescence method. *Indian J. Biochem. Biophys.* 34:307–312.

Hakansson, K., A. J. Doherty, S. Shuman, and D. B. Wigley. 1997. X-ray crystallography reveals a large conformational change during guanyl transfer by mRNA capping enzymes. *Cell.* 89:545–553.

Ishino, Y., H. Shinagawa, K. Makino, S. Tsunasawa, F. Sakiyama, and A. Nakata. 1986. Nucleotide sequence of the lig gene and primary structure of DNA ligase of *Escherichia coli*. *Mol. Gen. Genet.* 204:1–7.

Kaczorowski, T., and W. Szybalski. 1996. Co-operativity of hexamer ligation. *Gene.* 179:189–193.

Kube, D., T. V. Esakova, M. V. Ivanov, A. I. Gromov, and N. K. Nagradova. 1987. Detection of ligand-induced conformation changes in lactate dehydrogenase by using fluorescent probes. *Biokhimiia.* 52: 179–187.

Kuznetsova, I. M., O. V. Stepanenko, K. K. Turoverov, L. Zhu, J. M. Zhou, A. L. Fink, and V. N. Uversky. 2002. Unraveling multistate unfolding of rabbit muscle creatine kinase. *Biochim. Biophys. Acta.* 1596:138–155.

Lakowicz, J. 1983. Fluorescence quenching. *In* Principles of Fluorescence Spectroscopy. J. R. Lakowicz, editor. Plenum Press, New York. 257–301.

Lee, J. Y., C. Chang, H. K. Song, J. Moon, J. K. Yang, H. K. Kim, S. T. Kwon, and S. W. Suh. 2000. Crystal structure of NAD^+-dependent DNA ligase: modular architecture and functional implications. *EMBO J.* 19:1119–1129.

Lehman, I. R. 1974. DNA ligase: structure, mechanism, and function. *Science.* 186:790–797.

Levitt, M. 1992. Accurate modeling of protein conformation by automatic segment matching. *J. Mol. Biol.* 226:507–533.

Marchal, S., and G. Branlant. 1999. Evidence for the chemical activation of essential cys-302 upon cofactor binding to nonphosphorylating glyceraldehyde 3-phosphate dehydrogenase from *Streptococcus mutans*. *Biochemistry.* 38:12950–12958.

Martin, I. V., and S. A. MacNeill. 2002. ATP-dependent DNA ligases. *Genome Biol.* 3:3005.1–3005.7.

Matouschek, A., J. M. Matthews, C. M. Johnson, and A. R. Fersht. 1994. Extrapolation to water of kinetic and equilibrium data for the unfolding of barnase in urea solutions. *Protein Eng.* 7:1089–1095.

Mayr, L. M., and F. X. Schmid. 1993. Stabilization of a protein by guanidinium chloride. *Biochemistry.* 32:7994–7998.

Modrich, P., Y. Anraku, and I. R. Lehman. 1973. Deoxyribonucleic acid ligase. Isolation and physical characterization of the homogeneous enzyme from *Escherichia coli*. *J. Biol. Chem.* 248:7495–7501.

Morimatsu, K., T. Horii, and M. Takahashi. 1995. Interaction of Tyr103 and Tyr264 of the RecA protein with DNA and nucleotide cofactors.

Fluorescence study of engineered proteins. *Eur. J. Biochem.* 228:779–785.

Munishkina, L. A., C. Phelan, V. N. Uversky, and A. L. Fink. 2003. Conformational behavior and aggregation of a-synuclein in organic solvents: modeling the effects of membranes. *Biochemistry.* 42:2720–2730.

Murataliev, M. B., and R. Feyereisen. 2000. Functional interactions in cytochrome P450BM3. Evidence that NADP(H) binding controls redox potentials of the flavin cofactors. *Biochemistry.* 39:12699–12707.

Myers, J. K., C. N. Pace, and J. M. Scholtz. 1995. Denaturant m values and heat capacity changes: relation to changes in accessible surface areas of protein unfolding. *Protein Sci.* 4:2138–2148.

Pace, C. N. 1986. Determination and analysis of urea and guanidine hydrochloride denaturation curves. *Methods Enzymol.* 131:266–280.

Pace, C. N. 1990. Measuring and increasing protein stability. *Trends Biotechnol.* 8:93–98.

Panasenko, S. M., R. J. Alazard, and I. R. Lehman. 1978. A simple, three-step procedure for the large scale purification of DNA ligase from a hybrid lambda lysogen constructed *in vitro*. *J. Biol. Chem.*253:4590–4592.

Pearson, W. R. 1996. Effective protein sequence comparison. *Methods Enzymol.* 266:227–258.

Permyakov, E. A., V. V. Yarmolenko, V. I. Emelyanenko, E. A. Burstein, J. Closset, and C. Gerday. 1980. Fluorescence studies of the calcium binding to whiting (*Gadus merlangus*) parvalbumin. *Eur. J. Biochem.* 109:307–315.

Ptitsyn, O. B. 1995. Molten globule and protein folding. *Adv. Protein Chem.* 47:83–229.

Royer, C. A., C. J. Mann, and C. R. Matthews. 1993. Resolution of the fluorescence equilibrium unfolding profile of trp aporepressor using single tryptophan mutants. *Protein Sci.* 2:1844–1852.

Semisotnov, G. V., N. A. Rodionova, O. I. Razgulyaev, V. N. Uversky, A. F. Gripas, and R. I. Gilmanshin. 1991. Study of the ''molten globule'' intermediate state in protein folding by a hydrophobic fluorescent probe. *Biopolymers.* 31:119–128.

Shepherd, G. B., and G. G. Hammes. 1976. Fluorescence energy transfer measurements between ligand binding sites of the pyruvate dehydrogenase multienzyme complex. *Biochemistry.* 15:311–317.

Shuman, S. 1995. Vaccinia virus DNA ligase: specificity, fidelity, and inhibition. *Biochemistry.* 34:16138–16147.

Shuman, S., and B. Schwer. 1995. RNA capping enzyme and DNA ligase: a superfamily of covalent nucleotidyl transferases. *Mol. Microbiol.* 17:405–410.

Singleton, M. R., K. Hakansson, D. J. Timson, and D. B. Wigley. 1999. Structure of the adenylation domain of an NAD^+-dependent DNA ligase. *Structure.* 7:35–42.

Sinha, K. M., M. Ghosh, I. Das, and A. K. Datta. 1999. Molecular cloning and expression of adenosine kinase from *Leishmania donovani*: identification of unconventional P-loop motif. *Biochem. J.* 339:667–673.

Sriskanda, V., and S. Shuman. 2002. Conserved residues in domain Ia are required for the reaction of *Escherichia coli* DNA ligase with NAD^+. *J. Biol. Chem.* 277:9695–9700.

Takahashi, M., and T. Uchida. 1986. Thermophilic HB8 DNA ligase: effects of polyethylene glycols and polyamines on blunt-end ligation of DNA. *J. Biochem.* 100:123–131.

Tang, C. K., C. E. Jeffers, J. C. Nichols, and S. C. Tu. 2001. Flavin specificity and subunit interaction of *Vibrio fischeri* general NAD(P)H-flavin oxidoreductase FRG/FRase I. *Arch. Biochem. Biophys.* 392:110–116.

Thorbjarnardóttir, S. H., Z. O. Jónsson, O. S. Andresson, J. K. Kristjánsson, G. Eggertsson, and A. Pálsdóttir. 1995. Cloning and sequence analysis of the DNA ligase-encoding gene of *Rhodothermus marinus*, and over-production, purification and characterization of two thermophilic DNA ligases. *Gene.* 161:1–6.

Timson, D. J., M. R. Singleton, and D. B. Wigley. 2000. DNA ligases in the repair and replication of DNA. *Mutat. Res.* 460:301–318.

Timson, D. J., and D. B. Wigley. 1999. Functional domains of an NAD^+-dependent DNA ligase. *J. Mol. Biol.* 285:73–83.

Uversky, V. N. 1993. Use of fast protein size-exclusion liquid chromatography to study the unfolding of proteins which denature through the molten globule. *Biochemistry.* 32:13288–13298.

Uversky, V. N. 2002a. Cracking the folding code. Why do some proteins adopt partially folded conformations, whereas other don't? *FEBS Lett.* 514:181–183.

Uversky, V. N. 2002b. What does it mean to be natively unfolded? *Eur. J. Biochem.* 269:2–12.

Uversky, V. N., and A. L. Fink. 2002. The chicken-egg scenario of protein folding revisited. *FEBS Lett.* 515:79–83.

Uversky, V. N., L. N. Garriques, I. S. Millett, S. Frokjaer, J. Brange, S. Doniach, and A. L. Fink.2003. Prediction of the association state of insulin using spectral parameters. *J. Pharm. Sci.* 92:847–858.

Uversky, V. N., and O. B. Ptitsyn. 1994. Partly folded state, a new equilibrium state of protein molecules: four-state guanidinium chloride-induced unfolding of β-lactamase at low temperature. *Biochemistry.* 33:2782–2791.

Uversky, V. N., and O. B. Ptitsyn. 1996. Further evidence on the equilibrium ''pre-molten globule state'': four-state guanidinium chloride-induced unfolding of carbonic anhydrase B at low temperature. *J. Mol. Biol.* 255:215–228.

Vanhove, M., G. Guillaume, P. Ledent, J. H. Richards, R. H. Pain, and J. M. Frere. 1997. Kinetic and thermodynamic consequences of the removal of the Cys-77-Cys-123 disulphide bond for the folding of TEM-1 β-lactamase. *Biochem. J.* 321:413–417.

Vassilenko, K. S., and V. N. Uversky. 2002. Native-like secondary structure of molten globules. *Biochim. Biophys. Acta.* 1594:168–177.

Wilkinson, A., J. Day, and R. Bowater. 2001. Bacterial DNA ligases. *Mol. Microbiol.* 40:1241–1248.

Zimmerman, S. B., and B. H. Pheiffer. 1983. Macromolecular crowding allows blunt-end ligation by DNA ligases from rat liver or *Escherichia coli*. *Proc. Natl. Acad. Sci. USA.* 80:5852–5856.